J. Fluid Mech. (2023), *vol*. 977, A15, doi:10.1017/jfm.2023.983

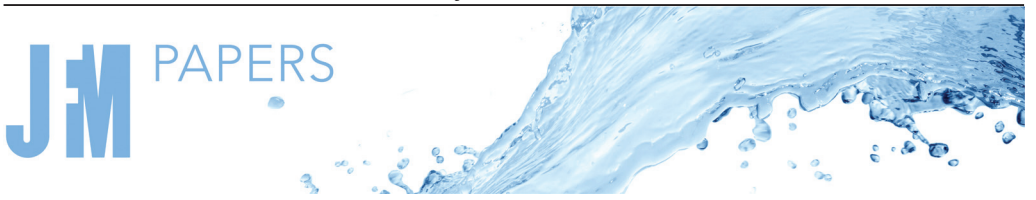

The '−1' decay law for some small-scale quantities at large Péclet numbers and fixed Reynolds numbers

S.L. Tang[1,†], R.A. Antonia[2] and L. Djenidi[3]

[1]Center for Turbulence Control, Harbin Institute of Technology, Shenzhen, 518055, PR China

[2]School of Engineering, University of Newcastle, NSW 2308, Australia

[3]Department of Mechanical Engineering, Indian Institute of Technology - Bombay, Powai, Mumbai 400076, India

(Received 28 March 2023; revised 16 October 2023; accepted 16 November 2023)

The effect of a uniform mean scalar gradient on the small scales of a passive scalar field in statistically stationary homogeneous isotropic turbulence is investigated through the transport equation for the scalar fluctuation. After some manipulation of the equation, it is shown that the effect can be recast in the form $S_\theta^* Pe_{\lambda_\theta}^{-1}$ (S_θ^* is the non-dimensional scalar gradient, Pe_{λ_θ} is the turbulent Péclet number). This effect gradually disappears as Pe_{λ_θ} becomes sufficiently large, implying a gradual approach towards local isotropy of the passive scalar. It is further argued that, for a given S_θ^*, the normalized odd moments of the scalar derivative tend towards isotropy as $Pe_{\lambda_\theta}^{-1}$. This is supported by direct numerical simulations data for the normalized odd moments of the scalar derivative at large Péclet numbers. Further, the present derivation leads to the same prediction ($\sim Sc^{-0.45}$ where Sc is the Schmidt number) as Buaria *et al.* (*Phys. Rev. Lett.*, vol. 126, no. 3, 2021*a*, p. 034504) and complements the derivation by the latter authors, which is based on dimensional arguments and the introduction of a new diffusive length scale.

Key words: turbulence theory

1. Introduction

The skewness of the scalar derivative S_3, defined as

$$S_m = \frac{\overline{\left(\dfrac{\partial\theta}{\partial x_1}\right)^m}}{\overline{\left(\dfrac{\partial\theta}{\partial x_1}\right)^2}^{m/2}}, \quad m = 3, \tag{1.1}$$

† Email address for correspondence: shunlin.tang88@gmail.com

where θ is the scalar fluctuation and m is a positive integer, is generally of order 1 when the Schmidt number $Sc(\equiv \nu/\kappa$, ν is the kinematic viscosity and κ is the diffusivity of the scalar) is of order 1 in shear flows such as wakes, jets and homogeneous shear flows (e.g. Mestayer *et al.* 1976; Gibson, Friehe & McConnell 1977). This has been interpreted as evidence that local isotropy of the passive scalar field is violated (e.g. Mestayer *et al.* 1976; Sreenivasan & Antonia 1977; Sreenivasan, Antonia & Britz 1979; Sreenivasan & Tavoularis 1980; Subramanian & Antonia 1982; Sreenivasan 1991; Holzer & Siggia 1994; Pumir 1994; Tong & Warhaft 1994; Sreenivasan & Antonia 1997; Shraiman & Siggia 2000; Warhaft 2000; Yeung, Xu & Sreenivasan 2002; Yeung, Donzis & Sreenivasan 2005; Monin & Yaglom 2007; Yeung & Sreenivasan 2014; Clay 2017; Sreenivasan 2019; Buaria *et al.* 2021*a*; Shete *et al.* 2022). On the other hand, there is evidence that, as Sc increases from approximately 10^{-3} to 10^3, $|S_3|$ along a direction parallel to the mean scalar gradient first increases before decreasing with increasing Sc (e.g. Yeung *et al.* 2002; Antonia & Orlandi 2003; Brethouwer, Hunt & Nieuwstadt 2003; Schumacher & Sreenivasan 2003; Yeung *et al.* 2004; Donzis, Sreenivasan & Yeung 2005; Yasuda *et al.* 2020; Buaria *et al.* 2021*a*; Shete *et al.* 2022). In particular, using dimensional arguments, Sreenivasan (2019), Buaria *et al.* (2021*a*) and Shete *et al.* (2022) derived relations for $|S_3|$, $|S_5|$ and $|S_7|$. Each of these quantities was found to decrease with Sc as $Sc^{-1/2}$ at a given Re_λ. However, this behaviour was not supported well by the direct numerical simulations (DNS) data of Buaria *et al.* (2021*a*) at $Re_\lambda = 140$ over a significant range $Sc(= 1\text{–}512)$. Here, Re_λ is the Taylor microscale Reynolds number defined by $\overline{u_1^2}^{1/2}\lambda/\nu$, where λ is the longitudinal Taylor microscale defined by $\lambda = \overline{u_1^2}^{1/2}/\overline{(\partial u_1/\partial x_1)^2}^{1/2}$ and u_i is the fluctuation velocity in the x_i direction. Further, Buaria *et al.* (2021*a*) introduced a new diffusive length scale in their dimensional analysis and obtained $\sim Sc^{-0.45}$, which is supported reasonably well by their DNS data for $Sc \gtrsim 4$. We recall that Obukhov (1949) and Corrsin (1951) assumed that the small scales of a passive scalar introduced in a turbulent flow are isotropic in space and stationary in time at sufficiently high Péclet numbers. In this paper, the turbulent Péclet number Pe_{λ_θ} is defined as

$$Pe_{\lambda_\theta} = \frac{\overline{u_1^2}^{1/2}\lambda_\theta}{\kappa}, \tag{1.2}$$

where λ_θ $(\equiv \overline{\theta^2}^{1/2}/\overline{(\partial\theta/\partial x_1)^2}^{1/2})$ is the Corrsin microscale. However, it is not clear whether the influence of large-scale forcing, such as that due to the action of the mean scalar gradient on the small-scale anisotropy, is negligible when the Péclet number is not sufficiently large. A knowledge of how and at what rate the small scales of a passive scalar approach isotropy with increasing Pe_{λ_θ} is of significant importance. For example, local isotropy can significantly simplify the modelling of small scales since one component is generally sufficient to represent all other components. Therefore, the main objective of this paper is to examine how small-scale anisotropy evolves as Pe_{λ_θ} increases. We first examine how large-scale forcing associated with the mean scalar gradient affects the local anisotropy of the passive scalar and how this anisotropy evolves with Pe_{λ_θ}. Then, the available data for $|S_3|$, $|S_5|$ and $|S_7|$ in the literature are interpreted in the light of the present results. In particular, the relations for $|S_3|$, $|S_5|$ and $|S_7|$, i.e. $\sim Sc^{-0.45}$, proposed by Buaria *et al.* (2021*a*), will be compared with the present results.

This paper is structured as follows. In § 2, we derive and test the relations between the large-scale forcing associated with the mean scalar gradient and the local anisotropy of the passive scalar. A comparison between the dependence of $|S_3|$, $|S_5|$ and $|S_7|$ on Sc, *viz.*

$\sim Sc^{-0.45}$ proposed by Buaria *et al.* (2021*a*), and the present results is discussed in § 3. Conclusions are given in § 4.

2. Theoretical considerations and discussions

The dynamical equation for the scalar fluctuation θ is given by Corrsin (1952) as

$$\frac{\partial \theta}{\partial t} + \bar{U}_j \frac{\partial \theta}{\partial x_j} + u_j \frac{\partial \Theta}{\partial x_j} + u_j \frac{\partial \theta}{\partial x_j} - \overline{u_j \frac{\partial \theta}{\partial x_j}} = \kappa \frac{\partial}{\partial x_j} \frac{\partial \theta}{\partial x_j}, \tag{2.1}$$

where Θ is the mean scalar; $\bar{U}_i$ is the mean velocity in the x_i direction. Sreenivasan & Tavoularis (1980) derived a transport equation for $\overline{(\partial\theta/\partial x_1)^3}$ in a steady, homogeneous shear flow with uniform mean velocity and scalar gradients in the x_2 direction ($\partial \bar{U}_1/\partial x_2 =$ const. and $\partial\Theta/\partial x_2 =$ const.). Using a similar procedure as Sreenivasan & Tavoularis (1980), we first differentiate (2.1) with respect to x_α ($\alpha = 1, 2, 3$), then multiply the resulting equation by $(\partial\theta/\partial x_\alpha)^n$ and finally take the average to obtain

$$\begin{aligned}
&\overline{\left(\frac{\partial \theta}{\partial x_\alpha}\right)^n \frac{\partial}{\partial x_\alpha}\frac{\partial \theta}{\partial t}} + \frac{\partial \bar{U}_j}{\partial x_\alpha}\overline{\left(\frac{\partial \theta}{\partial x_\alpha}\right)^n \frac{\partial \theta}{\partial x_j}} + \bar{U}_j \overline{\left(\frac{\partial \theta}{\partial x_\alpha}\right)^n \frac{\partial}{\partial x_\alpha}\frac{\partial \theta}{\partial x_j}} \\
&\quad + \overline{\left(\frac{\partial \theta}{\partial x_\alpha}\right)^n \frac{\partial u_j}{\partial x_\alpha}\frac{\partial \Theta}{\partial x_j}} + \overline{\left(\frac{\partial \theta}{\partial x_\alpha}\right)^n u_j \frac{\partial}{\partial x_\alpha}\frac{\partial \Theta}{\partial x_j}} + \overline{\left(\frac{\partial \theta}{\partial x_\alpha}\right)^n \frac{\partial u_j}{\partial x_\alpha}\frac{\partial \theta}{\partial x_j}} \\
&\quad + \overline{\left(\frac{\partial \theta}{\partial x_\alpha}\right)^n u_j \frac{\partial}{\partial x_\alpha}\frac{\partial \theta}{\partial x_j}} - \overline{\left(\frac{\partial \theta}{\partial x_\alpha}\right)^n \frac{\partial}{\partial x_\alpha} u_j \frac{\partial \theta}{\partial x_j}} = \kappa \overline{\left(\frac{\partial \theta}{\partial x_\alpha}\right)^n \frac{\partial}{\partial x_\alpha}\frac{\partial}{\partial x_j}\frac{\partial \theta}{\partial x_j}}.
\end{aligned} \tag{2.2}$$

Since we consider only the statistically stationary case, we have

$$\overline{\left(\frac{\partial \theta}{\partial x_\alpha}\right)^n \frac{\partial}{\partial x_\alpha}\frac{\partial \theta}{\partial t}} = \overline{\left(\frac{\partial \theta}{\partial x_\alpha}\right)^n \frac{\partial}{\partial t}\frac{\partial \theta}{\partial x_\alpha}} = \frac{1}{n+1}\frac{\partial}{\partial t}\overline{\left(\frac{\partial \theta}{\partial x_\alpha}\right)^{n+1}} = 0. \tag{2.3}$$

In this paper, we focus on the passive scalar field convected by statistically stationary homogeneous isotropic turbulence under a uniform mean scalar gradient in the x_1 direction ($\partial\Theta/\partial x_1$). Therefore, the last two terms on the first line and the second term on the second line of (2.2) can be ignored. Further, since the flow is homogeneous, we have

$$\overline{\left(\frac{\partial \theta}{\partial x_\alpha}\right)^n u_j \frac{\partial}{\partial x_\alpha}\frac{\partial \theta}{\partial x_j}} = \frac{1}{n+1}\frac{\partial}{\partial x_j}\overline{u_j \left(\frac{\partial \theta}{\partial x_\alpha}\right)^{n+1}} = 0, \tag{2.4}$$

$$\overline{\left(\frac{\partial \theta}{\partial x_\alpha}\right)^n \frac{\partial}{\partial x_\alpha} u_j \frac{\partial \theta}{\partial x_j}} = \overline{\left(\frac{\partial \theta}{\partial x_\alpha}\right)^n \frac{\partial}{\partial x_\alpha}\frac{\partial \overline{u_j \theta}}{\partial x_j}} = 0. \tag{2.5}$$

Finally, (2.2) reduces to

$$\overline{\left(\frac{\partial \theta}{\partial x_\alpha}\right)^n \frac{\partial u_1}{\partial x_\alpha}\frac{\partial \Theta}{\partial x_1}} = -\overline{\left(\frac{\partial \theta}{\partial x_\alpha}\right)^n \frac{\partial u_j}{\partial x_\alpha}\frac{\partial \theta}{\partial x_j}} + \kappa \overline{\left(\frac{\partial \theta}{\partial x_\alpha}\right)^n \frac{\partial}{\partial x_\alpha}\frac{\partial}{\partial x_j}\frac{\partial \theta}{\partial x_j}}. \tag{2.6}$$

The left-hand side term is the (large-scale) mean scalar-gradient production. The two terms on the right side are the small-scale terms, which can be interpreted as representing the production and destruction of $\overline{(\partial\theta/\partial x_\alpha)^{n+1}}$ respectively. Note that, when $\partial\Theta/\partial x_1 = 0$ and

$n = 1$, (2.6) is the stationary form of the equation for $\overline{(\partial\theta/\partial x_\alpha)^2}$ first written by Corrsin (1953). The equation, which contained both mean velocity and mean scalar-gradient terms, was tested by Abe, Antonia & Kawamura (2009) in a turbulent channel flow at different Reynolds numbers. Wyngaard (1971) considered (2.6) with $n = 1$. He interpreted the first term on the right side of (2.6) as the production rate of $\overline{(\partial\theta/\partial x_\alpha)^2}$ due to the stretching of the temperature field by the turbulent strain field, which is balanced by the molecular smoothing of the gradient temperature field. Since (2.6) contains both large- and small-scale terms, it can be used to quantify the effect of the large-scale forcing associated with the mean scalar gradient on small-scale quantities. When n is even and $\alpha = 2$ or 3, the first term in (2.6) is zero if local isotropy is satisfied since all combinations of the indices in $\overline{(\partial\theta/\partial x_\alpha)^n(\partial u_1/\partial x_\alpha)}$ will lead to the Kronecker delta $\delta_{1\alpha}$ ($\alpha = 2$ or 3) under the assumption of local isotropy. As an example, the first term in (2.6) for $\alpha = 2$ and $n = 2$ can be written as

$$\overline{\frac{\partial u_1}{\partial x_2}\frac{\partial\theta}{\partial x_2}\frac{\partial\theta}{\partial x_2}\frac{\partial\Theta}{\partial x_1}} = \frac{3}{4}\left(\delta_{12}\delta_{22} + \delta_{12}\delta_{22} - \frac{2}{3}\delta_{12}\delta_{22}\right)\overline{\frac{\partial u_1}{\partial x_1}\left(\frac{\partial\theta}{\partial x_1}\right)^2\frac{\partial\Theta}{\partial x_1}} = 0, \tag{2.7}$$

after using the isotropic form of a single-point fourth-order velocity derivative tensor $\overline{(\partial u_i/\partial x_j)(\partial\theta/\partial x_n)(\partial\theta/\partial x_m)}$ (e.g. Antonia & Browne 1983; Wyngaard 2010). When n is odd and $\alpha = 2$ or 3, the first term in (2.6) is also zero if local isotropy is satisfied since all combinations of the indices in $\overline{(\partial\theta/\partial x_\alpha)^n(\partial u_1/\partial x_\alpha)}$ will lead to the Kronecker delta $\delta_{1\alpha}$ ($\alpha = 2$ or 3) or the permutation symbol $\epsilon_{1\alpha\alpha}$ or $\epsilon_{\alpha\alpha\alpha}$ under the assumption of local isotropy. Therefore, in (2.6), we only consider the subscript $\alpha = 1$, which represents the direction of the mean scalar gradient. After normalization by $\overline{(\partial\theta/\partial x_1)^2}^{(n+1)/2}\overline{(\partial u_1/\partial x_1)^2}^{1/2}$, the first term in (2.6) becomes

$$\left.\begin{aligned}\frac{\overline{\left(\frac{\partial\theta}{\partial x_1}\right)^n\frac{\partial u_1}{\partial x_1}\frac{\partial\Theta}{\partial x_1}}}{\overline{(\partial\theta/\partial x_1)^2}^{(n+1)/2}\overline{(\partial u_1/\partial x_1)^2}^{1/2}} &= \frac{\overline{\left(\frac{\partial\theta}{\partial x_1}\right)^n\frac{\partial u_1}{\partial x_1}\frac{\partial\Theta}{\partial x_1}}}{\overline{(\partial\theta/\partial x_1)^2}^{n/2}\overline{(\partial u_1/\partial x_1)^2}^{1/2}\overline{(\partial\theta/\partial x_1)^2}^{1/2}}\\ \frac{R_n\frac{\partial\Theta}{\partial x_1}}{\overline{(\partial\theta/\partial x_1)^2}^{1/2}} = \frac{R_n 6\kappa\overline{\theta^2}^{1/2}\overline{u_1^2}^{1/2}\frac{\partial\Theta}{\partial x_1}\overline{\left(\frac{\partial\theta}{\partial x_1}\right)^2}^{1/2}}{\overline{\theta^2}^{1/2}\overline{u_1^2}^{1/2}6\kappa\overline{(\partial\theta/\partial x_1)^2}} &= \frac{6R_nS_\theta^*}{Pe_{\lambda_\theta}}\end{aligned}\right\}, \tag{2.8}$$

where Pe_{λ_θ} is defined in (1.2); S_θ^* is defined as

$$S_\theta^* = \frac{\overline{\theta^2}^{1/2}\overline{u_1^2}^{1/2}\frac{\partial\Theta}{\partial x_1}}{\bar{\varepsilon}_\theta}, \tag{2.9}$$

with $\bar{\varepsilon}_\theta = 6\kappa\overline{(\partial\theta/\partial x_1)^2}$; for convenience, we refer to S_θ^* as the non-dimensional scalar gradient. Here, R_n is the normalized correlation involving the streamwise derivative of θ and u_1, defined as

$$R_n = \frac{\overline{\left(\frac{\partial\theta}{\partial x_1}\right)^n\frac{\partial u_1}{\partial x_1}}}{\overline{(\partial\theta/\partial x_1)^2}^{n/2}\overline{(\partial u_1/\partial x_1)^2}^{1/2}}. \tag{2.10}$$

Finally, after normalization by $\overline{(\partial\theta/\partial x_1)^2}^{(n+1)/2}\overline{(\partial u_1/\partial x_1)^2}^{1/2}$, (2.6) for $\alpha = 1$ can be rewritten as

$$\frac{6R_nS_\theta^*}{Pe_{\lambda_\theta}} = A_n, \tag{2.11}$$

where A_n is defined as

$$A_n = \frac{-\overline{\left(\frac{\partial\theta}{\partial x_1}\right)^n \frac{\partial u_j}{\partial x_1}\frac{\partial\theta}{\partial x_j}} + \kappa\overline{\left(\frac{\partial\theta}{\partial x_1}\right)^n \frac{\partial}{\partial x_1}\frac{\partial}{\partial x_j}\frac{\partial\theta}{\partial x_j}}}{\overline{(\partial\theta/\partial x_1)^2}^{(n+1)/2}\overline{(\partial u_1/\partial x_1)^2}^{1/2}}. \tag{2.12}$$

The numerator of A_n is simply the right-hand side of (2.6) with $\alpha = 1$. In that respect, A_n represents the normalized sum of the production and destruction of $\overline{(\partial\theta/\partial x_1)^{n+1}}$. Some remarks are warranted on the use of $\overline{(\partial\theta/\partial x_1)^2}$, which is one of the three components in the full scalar dissipation rate defined as $2\kappa\overline{(\partial\theta/\partial x_i)^2}$, in equations (2.11) and (2.9). The values of $\overline{(\partial\theta/\partial x_i)^2}$ along the directions perpendicular to the mean scalar gradient, i.e. the x_2 and x_3 directions, should be equal because of the symmetry. On the other hand, Yeung *et al.* (2002) showed that the ratio of parallel-to-perpendicular scalar-gradient variances (i.e. $\overline{(\partial\theta/\partial x_1)^2}/\overline{(\partial\theta/\partial x_2)^2}$ and $\overline{(\partial\theta/\partial x_1)^2}/\overline{(\partial\theta/\partial x_3)^2}$) is close to unity (their table III or figure 11*a*). In particular, this ratio is equal to 1.05 at $Sc = 1$ and $Re_\lambda = 140$ and 240, respectively (their table III). This implies that local isotropy is satisfied adequately in the context of the ratio of parallel-to-perpendicular scalar-gradient variances in this flow and justifies the use of $\overline{(\partial\theta/\partial x_1)^2}$ in (2.11) and (2.9). It is worth mentioning that local isotropy does not require R_2, R_4 and R_6 in (2.11) to be zero. For example, R_2, the mixed velocity-scalar derivative skewness, represents the production of $\bar{\varepsilon}_\theta$ generated by stretching of the scalar field as a result of the turbulent strain rate. Further, for $n = 2, 4, 6$ and when local isotropy is satisfied, any combination of the indices in A_2, A_4 and A_6 will lead to a term involving the permutation symbols ϵ_{111}, ϵ_{11j} or ϵ_{1jj}, which are zero. Based on the above analysis, it can be concluded from (2.11) that, due to the presence of the mean shear, A_2, A_4 and A_6 may not be 0 at finite Pe_{λ_θ} and thus the flow is anisotropic in the context of A_2, A_4 and A_6. Therefore, (2.11) provides a relation between the mean scalar gradient and the local anisotropy. Namely, since, regardless of whether local isotropy is satisfied, the large-scale production term (the term on left-hand side of (2.11)) is non-zero and the corresponding small-scale terms (A_2, A_4 and A_6 in (2.11)) are zero when local isotropy is assumed, we can use (2.11) to quantify the effect of the large-scale forcing caused by the mean shear on the degree of isotropy of the small scales. Specifically, the relation shows how the level of local anisotropy depends on the magnitudes of S_θ^*, Pe_{λ_θ} and R_n for $n = 2, 4$ and 6. If $R_nS_\theta^*$ for $n = 2, 4, 6$ does not increase as rapidly as Pe_{λ_θ}, A_2, A_4 and A_6 should then go to zero when Pe_{λ_θ} is sufficiently large, irrespective of the magnitude of S_θ^*. In particular, for a given S_θ^*, if R_n for $n = 2, 4, 6$ are constant, A_n will behave as $Pe_{\lambda_\theta}^{-1}$ in statistically stationary homogeneous isotropic turbulence with a uniform mean scalar gradient. Figure 1(*a*) shows the distributions of S_θ^* and R_2 in statistically stationary homogeneous isotropic turbulence with a uniform mean scalar gradient at $Re_\lambda = 38$. We can observe that the magnitude of R_2 decreases slightly as Sc increases for $Sc \lesssim 10$ and appears to be approximately constant for $Sc \gtrsim 10$. Similarly, the magnitude of S_θ^* increases as Sc increases for $Sc \lesssim 10$ and also becomes approximately constant for $Sc \gtrsim 10$. We thus can conclude that A_2 should behave as $Pe_{\lambda_\theta}^{-1}$ for $Sc \gtrsim 10$. It is worth mentioning

that the values of R_4 and R_6 in this flow are not available. However, R_2, R_4 and R_6 can be related to the normalized high-order moments of scalar derivatives via the following Cauchy–Schwarz inequalities:

$$\overline{\left|\left(\frac{\partial\theta}{\partial x_1}\right)^2\frac{\partial u_1}{\partial x_1}\right|} \le \overline{\left(\frac{\partial\theta}{\partial x_1}\right)^4}^{1/2}\overline{\left(\frac{\partial u_1}{\partial x_1}\right)^2}^{1/2} \Rightarrow |R_2| \le \frac{\overline{(\partial\theta/\partial x_1)^4}^{1/2}}{\overline{(\partial\theta/\partial x_1)^2}} = F_{\|4}^{1/2}, \tag{2.13a}$$

$$\overline{\left|\left(\frac{\partial\theta}{\partial x_1}\right)^4\frac{\partial u_1}{\partial x_1}\right|} \le \overline{\left(\frac{\partial\theta}{\partial x_1}\right)^8}^{1/2}\overline{\left(\frac{\partial u_1}{\partial x_1}\right)^2}^{1/2} \Rightarrow |R_4| \le \frac{\overline{(\partial\theta/\partial x_1)^8}^{1/2}}{\overline{(\partial\theta/\partial x_1)^2}} = F_{\|8}^{1/2}, \tag{2.13b}$$

$$\overline{\left|\left(\frac{\partial\theta}{\partial x_1}\right)^6\frac{\partial u_1}{\partial x_1}\right|} \le \overline{\left(\frac{\partial\theta}{\partial x_1}\right)^{12}}^{1/2}\overline{\left(\frac{\partial u_1}{\partial x_1}\right)^2}^{1/2} \Rightarrow |R_6| \le \frac{\overline{(\partial\theta/\partial x_1)^{12}}^{1/2}}{\overline{(\partial\theta/\partial x_1)^2}^3} = F_{\|12}^{1/2}, \tag{2.13c}$$

where $F_{\|4}$, $F_{\|8}$ and $F_{\|12}$ are the normalized 4th, 8th and 12th moments of scalar derivatives along the direction parallel to the mean gradient. The inequalities in (2.13) imply that the magnitudes of R_2, R_4 and R_6 should not exceed those of $F_{\|4}$, $F_{\|8}$ and $F_{\|12}$. Figure 11(c) of Yeung *et al.* (2002) ($Sc = 0.25$–64) shows that the flatness of scalar derivatives along directions parallel ($F_{\|4}$) and perpendicular ($F_{\perp 4}$) to the mean gradient are approximately constant for $Sc > 10$ at $Re_\lambda = 38$. Also, at a higher $Re_\lambda (= 140)$, figure 8 of Buaria *et al.* (2021*a*) ($Sc = 1$–512) shows that the normalized 4th, 6th and 8th moments of scalar derivatives along directions parallel ($F_{\|4}$, $F_{\|6}$ and $F_{\|8}$) and perpendicular ($F_{\perp 4}$, $F_{\perp 6}$ and $F_{\perp 8}$) to the mean gradient approach each other and become independent of Sc for $Sc \gtrsim 8$. Based on this information, for the normalized moments of the scalar derivatives and the inequalities in (2.13), it seems reasonable to assume that R_4 and R_6 become independent of Sc, like R_2 (figure 1*a*), for $Sc > 10$. In this situation, we can conclude that A_4 and A_6, like A_2, should behave as $Pe_{\lambda_\theta}^{-1}$ for $Sc \gtrsim 10$.

We recall that $|S_3|$, $|S_5|$ and $|S_7|$ are frequently used to test local isotropy of a passive scalar. In this context, it is interesting to examine whether $|S_3|$, $|S_5|$ and $|S_7|$ will follow the prediction (2.11), equivalently whether $|S_3|$, $|S_5|$ and $|S_7|$ will follow $A_n \sim Pe_{\lambda_\theta}^{-1}$ for $n = 2, 4, 6$ for $Sc \gtrsim 10$. Although A_n and $|S_m|$ are different small-scale quantities, they have some features in common. For example, they both are strongly affected by the uniform mean scalar gradient; they both quantify the degree of local anisotropy of the passive scalar. Figure 1(b) shows the distributions of $|S_3|$, $|S_5|$ and $|S_7|$ vs Pe_{λ_θ}, using the data of Yeung *et al.* (2002). In order to obtain the values of Pe_{λ_θ}, we have used the following relation:

$$\frac{Pe_{\lambda_\theta}}{Re_\lambda} = \left(\frac{6ScR_\theta}{5}\right)^{1/2}, \tag{2.14}$$

where the time scale ratio R_θ can be rewritten as

$$R_\theta = \frac{\overline{\theta^2}/\bar{\varepsilon}_\theta}{\overline{q^2}/\bar{\varepsilon}} = \frac{\overline{\theta^2}\bar{\varepsilon}}{3\overline{u_1^2}\bar{\varepsilon}_\theta} = \frac{\dfrac{\bar{\varepsilon}L}{\overline{u_1^2}^{3/2}}}{\dfrac{3\bar{\varepsilon}_\theta L}{\overline{u_1^2}^{1/2}\,\overline{\theta^2}}} = \frac{C_\varepsilon}{3C_{\varepsilon\theta}}, \tag{2.15}$$

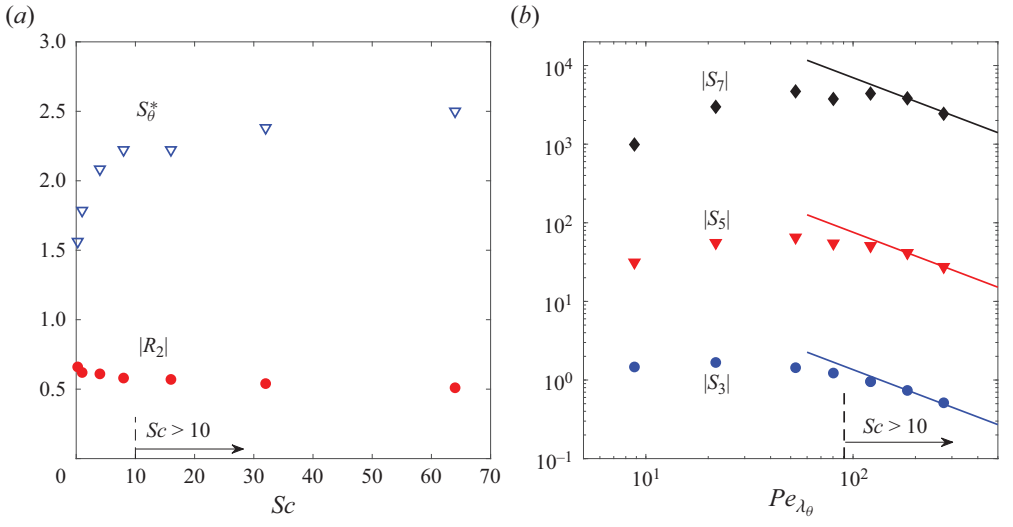

Figure 1. (*a*) Dependence of S_θ^* (∇, blue) and R_2 ($\bullet$, red) on Sc for $Re_\lambda = 38$. (*b*) Dependence of $|S_3|$ ($\bullet$, blue), $|S_5|$ ($\blacktriangledown$, red) and $|S_7|$ ($\blacklozenge$) at $Re_\lambda = 38$. Lines: $\sim Pe_{\lambda_\theta}^{-1}$. The horizontal arrows in (*a*) and (*b*) indicate the region in which $R_2 \approx const$ and $S_\theta^* \approx const$. To plot (*a*) and (*b*), we have used the DNS data of Yeung *et al.* (2002); see text for details.

where L is the integral length scale. The parameters C_ε and $C_{\varepsilon\theta}$ at Re_λ=38 and $Sc = 0.25$–64 are calculated from table 1 of Donzis *et al.* (2005). Note that, at $Pe_{\lambda_\theta} = 121$ (or equivalently $Sc = 16$), there are two values of $|S_m|$ at each m (=3,5,7) (see figure 12 of Yeung *et al.* 2002), corresponding to two simulations at different spatial resolutions, i.e. $k_{max}\eta_B = 1.48$ and 2.95 (see table I of Yeung *et al.* (2002); here, k_{max} is the resolved highest wavenumber and η_B is the Batchelor length scale). In figure 1(*b*), the values of $|S_m|$ at $k_{max}\eta_B = 1.48$ are not shown since small values of $k_{max}\eta_B$ would result in an underestimation of the magnitude of $|S_m|$; for example, this can be observed from table III of Yeung *et al.* (2002) in the context of $|S_3|$ and $|S_4|$ at $Sc = 16$. We can observe from figure 1(*b*) that $|S_3|$, $|S_5|$ and $|S_7|$ exhibit a tendency to behave as $Pe_{\lambda_\theta}^{-1}$ for $Sc > 10$ (or equivalently $Pe_{\lambda_\theta} > 91$). Namely, the flow approaches local isotropy as $Pe_{\lambda_\theta}^{-1}$ in the context of $|S_3|$, $|S_5|$ and $|S_7|$.

We now examine whether the behaviours of $|S_3|$, $|S_5|$ and $|S_7|$ follow the behaviours of A_2, A_4 and A_6 (or the prediction (2.11)) at $Re_\lambda = 140$. Buaria *et al.* (2021*b*) show that $C_{\varepsilon\theta}$ decreases as Sc increases from 1 to 512 at $Re_\lambda = 140$ (see their figure 2, which was digitized to replot $|S_3|$, $|S_5|$ and $|S_7|$ vs Pe_{λ_θ}). Figure 2 shows the distributions of $|S_3|$, $|S_5|$ and $|S_7|$ of Buaria *et al.* (2021*a*) as a function of Pe_{λ_θ}. To replot the data we used (2.14) and (2.15) with $C_\varepsilon = 0.46$ (estimated using data in table 1 of Donzis *et al.* (2005) at $Re_\lambda = 140$) and the values of $C_{\varepsilon\theta}$, the distributions of $|S_3|$, $|S_5|$ and $|S_7|$ vs Sc for the data of Buaria *et al.* (2021*a*) are replotted in figure 2 as a function of Pe_{λ_θ}. Figure 2 shows that $|S_3|$, $|S_5|$ and $|S_7|$ follow approximately the behaviour $Pe_{\lambda_\theta}^{-1}$ for $Sc > 10$ (or equivalently $Pe_{\lambda_\theta} > 257$). Namely, the flow approaches local isotropy as $Pe_{\lambda_\theta}^{-1}$ in the context of $|S_3|$, $|S_5|$ and $|S_7|$. We can observe that the behaviour of $|S_3|$, $|S_5|$ and $|S_7|$ for $Sc > 10$ in figures 1(*b*) and 2 is consistent with the prediction in (2.11).

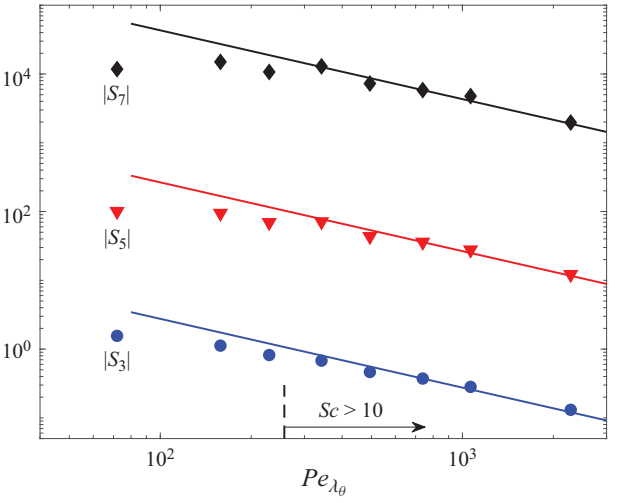

Figure 2. Dependence of $|S_3|$ (●, blue), $|S_5|$ (▼, red) and $|S_7|$ (♦) on Pe_{λ_θ} for $Re_\lambda = 140$. Lines: $\sim Pe_{\lambda_\theta}{}^{-1}$. The horizontal arrow indicates the region where $Sc > 10$, S_θ^* and $|R_2|$ are approximately constant and the normalized 4th, 6th and 8th moments of scalar derivatives along directions parallel and perpendicular to the mean gradient are also approximately constant. The symbols correspond to the DNS data of Buaria *et al.* (2021*a*).

3. Discussion

Using dimensional analysis, Sreenivasan (2019), Buaria *et al.* (2021*a*) and Shete *et al.* (2022) have derived relations for $|S_3|$, $|S_5|$ and $|S_7|$, i.e.

$$|S_m| \sim Sc^{-1/2}, \tag{3.1}$$

($m = 3, 5, 7$) at a given Re_λ. On the other hand, using (2.14) and (2.15), (2.11) can be rewritten as

$$A_n = \sqrt{90}\frac{R_n S_\theta^*}{Re_\lambda}\left(\frac{C_{\varepsilon\theta}}{ScC_\varepsilon}\right)^{1/2}. \tag{3.2}$$

We recall $|S_m| \sim A_n$ for $Sc > 10$ (figures 1*b* and 2). Equation (3.2) can be reduced to (3.1), provided R_n, S_θ^* and $C_{\varepsilon\theta}$ do not depend on Sc at a given Re_λ. As shown in figure 1(*a*), R_2 and S_θ^* are approximately constant for $Sc > 10$. However, the available data indicate that $C_{\varepsilon\theta}$ decreases as Sc increases at a given Re_λ (Buaria, Yeung & Sawford 2016; Buaria *et al.* 2021*b*). In particular, Buaria *et al.* (2021*b*) showed that there is an empirical relation for $C_{\varepsilon\theta}$ vs Sc, i.e. $C_{\varepsilon\theta} = 1/\log Sc$. They further showed that the $1/\log Sc$ dependence can be replaced by a weak power-law relation, i.e. $\sim Sc^{-0.1}$ (Buaria *et al.* 2021*a*). After introducing a new diffusive length scale in their dimensional analysis, they obtained

$$|S_m| \sim Sc^{-0.45}. \tag{3.3}$$

However, substituting $C_{\varepsilon\theta} \sim Sc^{-0.1}$ into (3.2), we obtain

$$A_n \sim Sc^{-0.55}, \tag{3.4}$$

which should be tenable for $Sc > 10$. We now plot $|S_m|$ ($m = 3, 5, 7$) vs Sc using the data of Buaria *et al.* (2021*a*) in figure 3. Also shown are the predictions of (3.3) and (3.4), i.e. $\sim Sc^{-0.45}$ and $\sim Sc^{-0.55}$. Overall, (3.3) seems to be superior to (3.4) when the three data points for $Sc < 10$ are included. However, since (3.4) only applies to the range $Sc > 10$,

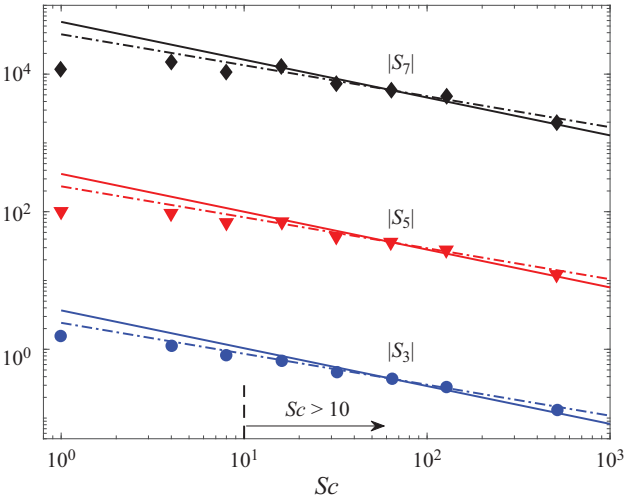

Figure 3. Dependence of $|S_3|$ (•, blue), $|S_5|$ (▼, red) and $|S_7|$ (♦) on Sc at $Re_\lambda = 140$. Solid Lines: $\sim Sc^{-0.55}$, i.e. the prediction of (3.4). Dash-dotted lines: $\sim Sc^{-0.45}$, i.e. the prediction of (3.3). The horizontal arrow indicates the region where $Sc > 10$, S_θ^* and $|R_2|$ are approximately constant and the normalized 4th, 6th and 8th moments of scalar derivatives along directions parallel and perpendicular to the mean gradient are also approximately constant. The symbols correspond to the DNS data of Buaria *et al.* (2021*a*).

we can conclude that both (3.3) and (3.4) provide similarly adequate descriptions of the data when $Sc > 10$.

It is of interest to explain the difference between the predictions of (3.3) and (3.4), i.e. $\sim Sc^{-0.45}$ and $\sim Sc^{-0.55}$ for $Sc < 10$. We can observe from figure 1(*a*) that the variation of $|R_2|$ in the range $Sc = 1$–10 is actually very small. However, the magnitude of S_θ^* increases from 1.78 to 2.22 when Sc increases from 1 to 8 at $Re_\lambda = 38$ (figure 1*a*); the magnitude of S_θ^* appears to be independent of Re_λ, at least for $Sc = 1$ (figure 4*a*). In order to take into account the impact of the variation of S_θ^* at low Sc on (3.2), a power-law fit is used to the data of S_θ^* at $Re_\lambda = 38$, 140 and 240. This fit is $S_\theta^* = 1.79Sc^{0.1}$ (figure 4*a*). Note that, here, we are mainly interested in the range $Sc = 1$–10. As discussed in the context of figure 1(*a*), S_θ^* is approximately constant for $Sc = 10$–64 (see also the blue symbols in figure 4*a*). Substituting $C_{\varepsilon\theta} \sim Sc^{-0.1}$ (see the discussion in the context of (3.3) or Buaria *et al.* 2021*a*) and $S_\theta^* = 1.79Sc^{0.1}$ in (3.2), we obtain

$$A_n \sim Sc^{-0.45}, \tag{3.5}$$

which is exactly the same as the prediction of (3.3), i.e. $\sim Sc^{-0.45}$ proposed by Buaria *et al.* (2021*a*). A possible reason why the approach of Buaria *et al.* (2021*a*) and the present approach lead to the same prediction may be as follows. One of the key ingredients of the present approach is the use of the turbulent Péclet number Pe_{λ_θ}, defined in (1.2), which can be written as a function of Re_λ, Sc, C_ε and $C_{\varepsilon\theta}$ (see (2.14) and (2.15)). Combining (1.2), (2.14) and (2.15), we can obtain

$$Pe_{\lambda_\theta} = \frac{\overline{u_1^2}^{1/2}\lambda_\theta}{\kappa} = \frac{\overline{u_1^2}^{1/2}\lambda\nu\lambda_\theta}{\kappa\nu\lambda} = Re_\lambda Sc\frac{\lambda_\theta}{\lambda} = Re_\lambda\left(\frac{6ScR_\theta}{5}\right)^{1/2} = Re_\lambda\left(\frac{2ScC_\varepsilon}{5C_{\varepsilon\theta}}\right)^{1/2}, \tag{3.6}$$

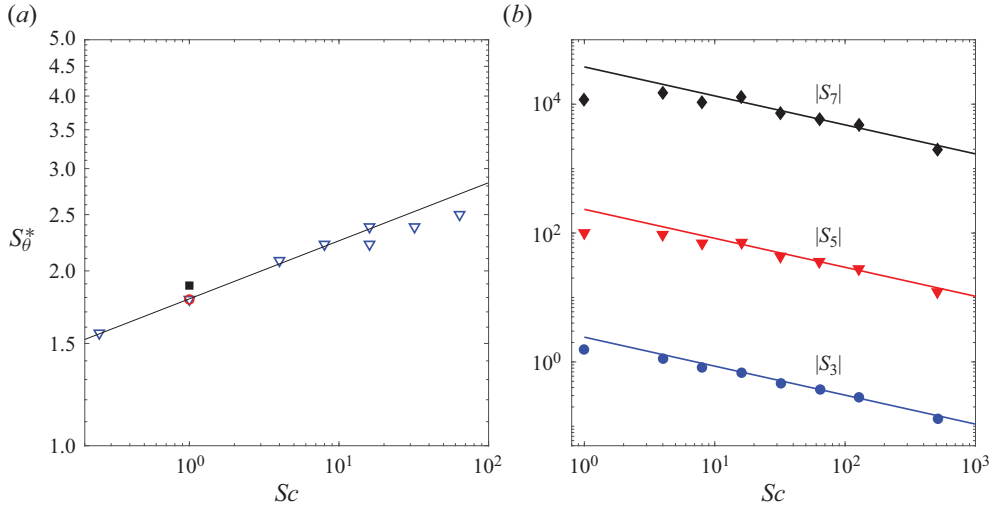

Figure 4. (*a*) Dependence of S_θ^* on Sc at $Re_\lambda = 38$ ($\bigtriangledown$, blue), 140 (■) and 240 (○, red). Solid line: $1.79Sc^{0.1}$. The symbols correspond to the DNS data of Yeung *et al.* (2002). (*b*) Dependence of $|S_3|$ (●, blue), $|S_5|$ (▼, red) and $|S_7|$ (♦) on Sc at $Re_\lambda = 140$. Solid lines: $\sim Sc^{-0.45}$, i.e. the prediction of (3.5). The symbols correspond to the DNS data of Buaria *et al.* (2021*a*).

which leads to

$$\frac{\lambda_\theta}{\lambda} = \left(\frac{2C_\varepsilon}{5ScC_{\varepsilon\theta}}\right)^{1/2} \approx \left(\frac{2C_\varepsilon}{5Sc0.69Sc^{-0.1}}\right)^{1/2} = \left(\frac{2C_\varepsilon}{3.45}\right)^{1/2} Sc^{-0.45} = 0.52Sc^{-0.45}. \tag{3.7}$$

The relations $C_{\varepsilon\theta} \approx 0.69Sc^{-0.1}$ (estimated from figure 2 of Buaria *et al.* 2021*b*) and $C_\varepsilon = 0.475$ (Yeung & Zhou 1997) at $Re_\lambda = 140$ have been used in (3.7). Equation (3.7) indicates that λ_θ/λ should decrease as Sc increases. Further, substituting (3.7) into the fourth term of (3.6) leads to $Pe_{\lambda_\theta} \approx 0.52Re_\lambda Sc^{0.55}$. Evidently, Pe_{λ_θ} is a function of Re_λ and Sc; a large Pe_{λ_θ} can be obtained either by increasing Sc at a fixed Re_λ or by increasing Re_λ at a fixed Sc. The isotropic relation between λ and η is $\lambda/\eta = 15^{1/4}Re_\lambda^{1/2}$. Using this relation, (3.7) can be further written as

$$\lambda_\theta \approx 0.52Sc^{-0.45}\lambda = Sc^{-0.45}Re_\lambda^{1/2}\eta. \tag{3.8}$$

On the other hand, the key ingredient in Buaria *et al.* (2021*a*) is the introduction of a new diffusive length scale, i.e. $\eta_D = \eta Sc^{-0.45}$ (see their (4)). Therefore, $\lambda_\theta = \eta_D$ only when $Re_\lambda = 1$. However, it is interesting to note $\lambda_\theta \sim \eta_D$ at any given Re_λ; this is a possible reason why both Buaria *et al.* (2021*a*) and the present approach lead to the same prediction.

We conclude this section by examining the data of Shete *et al.* (2022) at much higher $Re_\lambda (= 633)$ and $Sc = 0.1$, 0.7, 1 and 7. Since the maximum value of $Sc (= 7)$ is relatively low, we here only test the prediction of (3.5) which includes the variation of S_θ^* at low Sc. It can be observed from figure 5(*a*) that (3.5) is satisfied approximately for $Sc \gtrsim 0.7$. As was discussed in the context of figure 4(*b*), the prediction of (3.3) is the same as that of (3.5). It is worth mentioning that Buaria & Sreenivasan (2023) further examined the prediction of (3.3) in the context of $|S_3|$, i.e. $|S_3| \sim Sc^{-0.45}$, at $Re_\lambda = 140$, 390 and 633 and found that $|S_3| \sim Sc^{-0.45}$ is satisfied approximately for $Sc \gtrsim 3$ at all Re_λ (see their

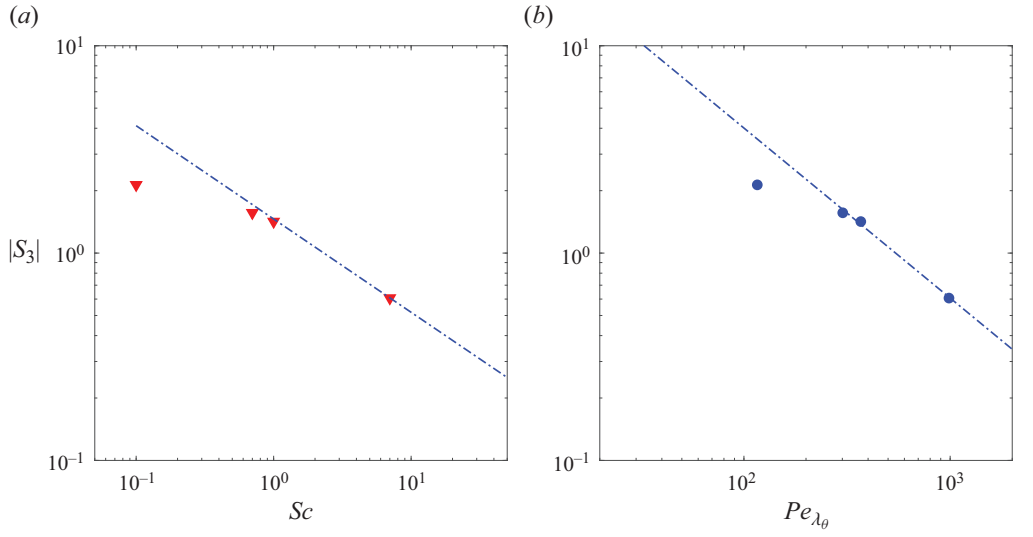

Figure 5. (*a*) Dependence of $|S_3|$ on Sc for $Re_\lambda = 633$. Line: $1.46Sc^{-0.45}$, i.e. the prediction of (3.5). (*b*) Dependence of $|S_3|$ on Pe_{λ_θ} at $Re_\lambda = 633$. Line: $175Pe_{\lambda_\theta}^{-0.82}$, i.e. the prediction of (3.10). The symbols in (*a*, *b*) correspond to the DNS data of Shete *et al.* (2022).

figure 1). Further, substituting $S_\theta^* = 1.79Sc^{0.1}$ into (2.11) leads to

$$A_n = \frac{6R_nS_\theta^*}{Pe_{\lambda_\theta}} = \frac{6R_n1.79Sc^{0.1}}{Pe_{\lambda_\theta}} \approx \frac{6R_n1.79}{Pe_{\lambda_\theta}}\left(\frac{Pe_{\lambda_\theta}}{0.52Re_\lambda}\right)^{0.1/0.55} \approx \frac{12.1R_n}{Re_\lambda^{0.18}}Pe_{\lambda_\theta}^{-0.82}. \quad (3.9)$$

We have used the relation $Pe_{\lambda_\theta} \approx 0.52Re_\lambda Sc^{0.55}$ (see the discussion in the context of (3.6) and (3.7)) in the third step of (3.9). At any given Re_λ, (3.9) can be simplified as

$$A_n \sim Pe_{\lambda_\theta}^{-0.82}. \quad (3.10)$$

Figure 5(*b*) shows that (3.10) is satisfied adequately for $Pe_{\lambda_\theta} \gtrsim 300$ (or equivalently for $Sc \gtrsim 0.7$). It should be pointed out that all the data we used for our study were digitized from figures presented in Yeung *et al.* (2002), Buaria *et al.* (2021*a*) and Shete *et al.* (2022). Since all the DNS data reported here have already been published, the reader can find detailed descriptions of the simulation such as the spatial resolution in the original papers. We stress that the present paper focuses only on the Pe_{λ_θ} variation with Sc at several fixed Re_λ, as shown in figure 1(*b*) ($Re_\lambda = 38$), figure 2 ($Re_\lambda = 144$) and figure 5(*b*) ($Re_\lambda = 633$). We do not assess any variation of small-scale quantities with Re_λ at fixed Sc; this merits further investigation.

4. Conclusions

Starting with the scalar transport equation for statistically stationary homogeneous isotropic turbulence with a uniform mean scalar gradient, we derived an expression for describing the relationship between the large-scale forcing associated with the mean scalar gradient and small-scale anisotropy reflected in the sum of the production and destruction of $\overline{(\partial\theta/\partial x_1)^{n+1}}$; this sum is denoted A_n for convenience (see (2.12)). The departure of the scalar field from local isotropy due to the (large-scale) production arising from the mean

scalar gradient (whose normalized expression is denoted S_θ^*) can be quantified through (2.11). The effect of S_θ^* on local anisotropy can be recast in the form $R_n S_\theta^* / Pe_{\lambda_\theta}^{-1}$ for $n = 2, 4, 6$. Since the available data show R_2, S_θ^* and the normalized 4th, 6th and 8th moments of scalar derivatives are approximately constant for $Sc \gtrsim 10$, it is expected that, in the context of A_2, A_4 and A_6, the small scales of the passive scalar field will approach isotropy as rapidly as $Pe_{\lambda_\theta}^{-1}$ approaches zero. This is fully consistent with the DNS data for $|S_3|$, $|S_5|$ and $|S_7|$ vs Pe_{λ_θ} for $Sc > 10$. This -1 power-law decay for the normalized odd moments of the scalar derivative $|S_3|$, $|S_5|$ and $|S_7|$ can be rewritten as a function of Sc, i.e. (3.4). Since $|S_m| \sim A_n$ for $Sc > 10$ (figures 1*b* and 2), it is found that both (3.3) and (3.4) provide similarly adequate descriptions of $|S_m|$ ($m = 3, 5, 7$) when $Sc > 10$ (figure 3). When the variation of S_θ^*, mainly in the range $Sc = 1$–10, is taken into account, the resulting prediction ($\sim Sc^{-0.45}$, or (3.5)) is the same as that of Buaria *et al.* (2021*a*) ($\sim Sc^{-0.45}$, or (3.3)). Further, the present approach complements that of Buaria *et al.* (2021*a*) who used dimensional arguments and introduced a new diffusive length scale.

Acknowledgements. S.L.T. thanks Professor M. de Bruyn Kops for the DNS data. We also thank Professor K.R. Sreenivasan for his constructive comments.

Funding. This research was supported by the National Natural Science Foundation of China (project no. 91952109), Guangdong Basic and Applied Basic Research Foundation (project no. 2023B1515020069) and Shenzhen Science and Technology Program (project nos. RCYX20210706092046085 and GXWD20220817171516009).

Declaration of interests. The authors report no conflict of interest.

Author ORCIDs.
S.L. Tang https://orcid.org/0000-0001-6379-8505;
L. Djenidi https://orcid.org/0000-0001-8614-3595.

References

Abe, H., Antonia, R.A. & Kawamura, H. 2009 Correlation between small-scale velocity and scalar fluctuations in a turbulent channel flow. *J. Fluid Mech.* **627**, 1–32.

Antonia, R.A. & Browne, L.W.B. 1983 The destruction of temperature fluctuations in a turbulent plane jet. *J. Fluid Mech.* **134**, 67–83.

Antonia, R.A. & Orlandi, P. 2003 Effect of Schmidt number on small-scale passive scalar turbulence. *Appl. Mech. Rev.* **56** (6), 615–632.

Brethouwer, G., Hunt, J.C.R. & Nieuwstadt, F.T.M. 2003 Micro-structure and Lagrangian statistics of the scalar field with a mean gradient in isotropic turbulence. *J. Fluid Mech.* **474**, 193–225.

Buaria, D., Clay, M.P., Sreenivasan, K.R. & Yeung, P.K. 2021*a* Small-scale isotropy and ramp-cliff structures in scalar turbulence. *Phys. Rev. Lett.* **126** (3), 034504.

Buaria, D., Clay, M.P., Sreenivasan, K.R. & Yeung, P.K. 2021*b* Turbulence is an ineffective mixer when Schmidt numbers are large. *Phys. Rev. Lett.* **126** (7), 074501.

Buaria, D. & Sreenivasan, K.R. 2023 Comparing velocity and passive scalar statistics in fluid turbulence at high Schmidt numbers and Reynolds numbers. arXiv:2302.05503.

Buaria, D., Yeung, P.K. & Sawford, B.L. 2016 A Lagrangian study of turbulent mixing: forward and backward dispersion of molecular trajectories in isotropic turbulence. *J. Fluid Mech.* **799**, 352–382.

Clay, M. 2017 Strained turbulence and low-diffusivity turbulent mixing using high performance computing. PhD thesis, Georgia Institute of Technology.

Corrsin, S. 1951 On the spectrum of isotropic temperature fluctuations in an isotropic turbulence. *J. Appl. Phys.* **22**, 469–473.

Corrsin, S. 1952 Heat transfer in isotropic turbulence. *J. Appl. Phys.* **23** (1), 113–118.

Corrsin, S. 1953 Remarks on turbulent heat transfer: an account of some features of the phenomenon in fully turbulent regions. In *Proceedings of the first Iowa Thermodynamics Symposium*, pp. 5–30. State University of Iowa.

DONZIS, D.A., SREENIVASAN, K.R. & YEUNG, P.K. 2005 Scalar dissipation rate and dissipative anomaly in isotropic turbulence. *J. Fluid Mech.* **532**, 199–216.

GIBSON, C.H., FRIEHE, C.A. & MCCONNELL, S.O. 1977 Structure of sheared turbulent fields. *Phys. Fluids* **20**, S156–S167.

HOLZER, M. & SIGGIA, E.D. 1994 Turbulent mixing of a passive scalar. *Phys. Fluids* **6** (5), 1820–1837.

MESTAYER, P.G., GIBSON, C.H., COANTIC, M.F. & PATEL, A.S. 1976 Local anisotropy in heated and cooled turbulent boundary layers. *Phys. Fluids* **19**, 1279–1287.

MONIN, A.S. & YAGLOM, A.M. 2007 *Statistical Fluid Dynamics*, vol. 2. MIT.

OBUKHOV, A.M. 1949 Structure of the temperature field in turbulent flows. *Izv. Akad. Nauk SSSR Geogr. Geofiz* **13**, 58–69.

PUMIR, A. 1994 A numerical study of the mixing of a passive scalar in three dimensions in the presence of a mean gradient. *Phys. Fluids* **6** (6), 2118–2132.

SCHUMACHER, J. & SREENIVASAN, K.R. 2003 Geometric features of the mixing of passive scalars at high Schmidt numbers. *Phys. Rev. Lett.* **91** (17), 174501.

SHETE, K.P., BOUCHER, D.J., RILEY, J.J. & DE BRUYN KOPS, S.M. 2022 Effect of viscous-convective subrange on passive scalar statistics at high Reynolds number. *Phys. Rev. Fluids* **7** (2), 024601.

SHRAIMAN, B.I. & SIGGIA, E.D. 2000 Scalar turbulence. *Nature* **405** (6787), 639–646.

SREENIVASAN, K. 1991 On local isotropy of passive scalars in turbulent shear flows. *Proc. R. Soc. Lond.* A **434**, 165–182.

SREENIVASAN, K.R. 2019 Turbulent mixing: a perspective. *Proc. Natl Acad. Sci.* **116** (37), 18175–18183.

SREENIVASAN, K.R. & ANTONIA, R.A. 1977 Skewness of temperature derivatives in turbulent shear flows. *Phys. Fluids* **20** (12), 1986–1988.

SREENIVASAN, K. & ANTONIA, R.A. 1997 The phenomenology of small-scale turbulence. *Annu. Rev. Fluid Mech.* **29**, 435–472.

SREENIVASAN, K.R., ANTONIA, R.A. & BRITZ, D. 1979 Local isotropy and large structures in a heated turbulent jet. *J. Fluid Mech.* **94** (4), 745–775.

SREENIVASAN, K.R. & TAVOULARIS, S. 1980 On the skewness of the temperature derivative in turbulent flows. *J. Fluid Mech.* **101** (4), 783–795.

SUBRAMANIAN, C.S. & ANTONIA, R.A. 1982 A model for the skewness of the temperature derivative in a turbulent boundary layer. *Phys. Fluids* **25**, 957–958.

TONG, C. & WARHAFT, Z. 1994 On passive scalar derivative statistics in grid turbulence. *Phys. Fluids* **6** (6), 2165–2176.

WARHAFT, Z. 2000 Passive scalars in turbulent flows. *Annu. Rev. Fluid Mech.* **32**, 203–240.

WYNGAARD, J.C. 1971 The effect of velocity sensitivity on temperature derivative statistics in isotropic turbulence. *J. Fluid Mech.* **48**, 763–769.

WYNGAARD, J.C. 2010 *Turbulence in the Atmosphere*. Cambridge University Press.

YASUDA, T., GOTOH, T., WATANABE, T. & SAITO, I. 2020 Péclet-number dependence of small-scale anisotropy of passive scalar fluctuations under a uniform mean gradient in isotropic turbulence. *J. Fluid Mech.* **898**, A4.

YEUNG, P.K., DONZIS, D.A. & SREENIVASAN, K.R. 2005 High-Reynolds-number simulation of turbulent mixing. *Phys. Fluids* **17**, 081703.

YEUNG, P.K. & SREENIVASAN, K.R. 2014 Direct numerical simulation of turbulent mixing at very low Schmidt number with a uniform mean gradient. *Phys. Fluids* **26** (1), 015107.

YEUNG, P.K., XU, S., DONZIS, D.A. & SREENIVASAN, K.R. 2004 Simulations of three-dimensional turbulent mixing for Schmidt numbers of the order 1000. *Flow Turbul. Combust.* **72** (2), 333–347.

YEUNG, P.K., XU, S. & SREENIVASAN, K.R. 2002 Schmidt number effects on turbulent transport with uniform mean scalar gradient. *Phys. Fluids* **14** (12), 4178–4191.

YEUNG, P.K. & ZHOU, Y. 1997 Universality of the Kolmogorov constant in numerical simulations of turbulence. *Phys. Rev.* E **56**, 1746–1752.